crystals

MDPI

Article

Micro-Structure and Dielectric Properties of $Ti_3C_2T_x$ MXene after Annealing Treatment under Inert Gases

Zhiwei Liu, Zhaobo Liu, Guanlong Li, Yan Zhao *, Kai Wang * and Xiangbao Chen

School of Materials Science and Engineering, Beihang University, Beijing 100191, China; lzwbuaa@163.com (Z.L.); lzbbuaa@163.com (Z.L.); 1601lgl@buaa.edu.cn (G.L.)

* Correspondence: jennyzhaoyan@buaa.edu.cn (Y.Z.); wangkai@buaa.edu.cn (K.W.)

Abstract: At present, the rapid development of electronic devices such as batteries, sensors, capacitors and so on is creating a huge demand for lightweight materials with a designed structure and function. $Ti_3C_2T_x$ MXene, a lightweight two-dimensional (2D) nanomaterial with excellent electronic properties, has been favored in this field. In this work, $Ti_3C_2T_x$ MXene was annealed under an inert gas (N_2, Ar and CO_2) atmosphere to design the crystal structure and interface of the nanosheets, and then the modified nanosheets with specific changes in dielectric properties were obtained. Among them, the key temperature points (100 °C, 300 °C, 500 °C and 800 °C) in the thermogravimetric (TG) test under an air atmosphere were used as the annealing temperature. When annealing under an air atmosphere, with the increase in temperature, the Ti layer gradually oxidized and evaporated, and the original two-dimensional structure was partly destroyed with some of the C atoms reacting with O_2 to form CO_2. In the inert gas atmosphere, however, the 2D structure is preserved, except that the surface end groups and layer spacing are changed. In addition, some N element doping was introduced into the nanosheets after N_2 atmosphere treatment, which changed the original lattice structure. After the Ar atmosphere treatment, some Ti atoms on the surface were oxidized in situ to form TiO_2 grains with different crystal forms, which increased the interfacial area. The C-TiO_2 structure of the nanosheets was more complete after treatment with the CO_2 atmosphere. All the nanosheets after heat treatment with an inert gas atmosphere retained the characteristic morphology of 2D materials, and different changes in the micro-structure caused changes in dielectric properties, thereby meeting the needs of 2D nanomaterials $Ti_3C_2T_x$ MXene in different scenarios.

Keywords: inert gases; crystal structure; dielectric property; 2D nanosheets

check for updates

Citation: Liu, Z.; Liu, Z.; Li, G.; Zhao, Y.; Wang, K.; Chen, X. Micro-Structure and Dielectric Properties of $Ti_3C_2T_x$ MXene after Annealing Treatment under Inert Gases. *Crystals* **2023**, *13*, 1234. https://doi.org/10.3390/cryst13081234

Academic Editor: Igor Yurkevich

Received: 24 July 2023
Revised: 5 August 2023
Accepted: 9 August 2023
Published: 10 August 2023

Copyright: © 2023 by the authors. Licensee MDPI, Basel, Switzerland. This article is an open access article distributed under the terms and conditions of the Creative Commons Attribution (CC BY) license (https://creativecommons.org/licenses/by/4.0/).

1. Introduction

At present, the rapid development of electronic devices such as sensors [1], batteries [2,3], capacitors [4] and so on is creating a huge demand for lightweight materials with a designed structure and function. Due to the high density, single structure and poor designability, the material system based on traditional metals has been unable to fulfill the application requirements of high integration and multi-function. Intelligent responsive materials, micro/nano devices and integrated circuit science put forward higher requirements for the scale and electronic properties of materials [5].

On this basis, more and more studies have been conducted on nanomaterials such as one-dimensional (1D) silver nanowire (AgNW) [6], carbon nanotubes (CNTs) [7,8], two-dimensional (2D) graphene [9,10], MXene [11–13] and MoS_2 [14,15]. In recent years, due to their good combination of physical and chemical properties such as high electron mobility, large specific surface area and good chemical stability, more and more research has focused on 2D carbon nanomaterials such as graphene, C_3N_4 and MXene. Similar to graphene, MXene exhibits high carrier densities and good electrical conductivities, especially the designability of surface groups [16].

It is well known that the MXene surface obtained by the current general HF and LiF-HCl etching method contains a large number of -OH, -F, -O and other functional groups [17].

Some reports show that these end groups have an impact on the electrical properties of MXenes such as conductivity, electron mobility and dielectric properties, which then affect the application [18,19]. Therefore, in order to change the electrical properties, the end group can be postprocessed by a series of treatment methods, such as changing the temperature, changing the acid–base environment and changing the atmosphere. For example, using density functional theory computation, Tang et al. [20] calculated that the elimination of MXenes' surface terminations improved its electrical conductivity while showing weak magnetic properties. In terms of dielectric properties, Tu et al. [21] reported that with the increase in the surface end groups on the MXene surface (for example, -O, -F and -OH), the dielectric permittivity of MXene/poly(vinylidene fluoride-trifluoro-ethylene-chlorofluoroehylene) composite showed an upward trend. Annealing treatment is one of the common methods in the preparation and modification of materials. The micro-structure of the material is changed via heating, and then its properties are designed. Since MXene is a carbon-based material, the traditional way of heat treatment in an air atmosphere obviously cannot be used for MXene modification. Therefore, it is important to study the annealing process of MXene under inert protective gas.

In this work, $Ti_3C_2T_x$ MXene was annealed under an inert gas (N_2, Ar and CO_2) atmosphere to design the crystal structure and interface of the nanosheets, and then the modified nanosheets with specific changes in dielectric properties were obtained. Among them, the key temperature points (100 °C, 300 °C, 500 °C and 800 °C) in the thermogravimetric (TG) test under an air atmosphere were used as the annealing temperature. In the inert gas atmosphere, the 2D structure is preserved, except that the surface end groups and layer spacing are changed. In addition, some N element doping was introduced into the nanosheets after N_2 atmosphere treatment, which changed the original lattice structure. After the Ar atmosphere treatment, some Ti atoms on the surface were oxidized in situ to form TiO_2 grains with different crystal forms, which increased the interfacial area. The C-TiO_2 structure of the nanosheets was more complete after treatment with the CO_2 atmosphere. All the nanosheets after heat treatment with an inert gas atmosphere retained the characteristic morphology of 2D materials, and different changes in the micro-structure caused changes in dielectric properties, thereby meeting the needs of 2D nanomaterials $Ti_3C_2T_x$ MXene in different scenarios.

2. Materials and Methods

2.1. Materials

Titanium Aluminum Carbide powders (Ti_3AlC_2, 400 mesh, purity of 98%, 11 technology Co., Ltd., Changchun, China), Hydrochloric acid (HCl, 36–38%, Modern Oriental (Beijing) Technology Development Co., Ltd., Beijing, China), Lithium fluoride (LiF, purity of 99%, Shanghai Aladdin Biochemical Technology Co., Ltd., Shanghai, China) and paraffin wax were obtained.

2.2. Preparation of $Ti_3C_2T_x$ MXene

Similar to the previous studies [17], using the liquid phase etching method, $Ti_3C_2T_x$ MXene nanosheets were prepared. Specifically, 1 g of LiF was added to 20 mL of 9 M HCl solution and stirred in an ice-water bath at 0 °C for 15 min. Then, 1 g of Ti_3AlC_2 MAX was slowly added over 10 min, the reaction was carried out at 45 °C for 45 h, and the reaction products were washed 6–7 times with deoxygenated water until the pH value approached 7. Finally, the $Ti_3C_2T_x$ MXene with a few-layered structure was obtained by sonicating for 60 min under Ar flow to prevent the MXene sheet structure from being oxidized and destroyed. The MXene dispersion obtained via ultrasound was freeze-dried for 72 h to get dry and pure MXene nanoplate powder.

2.3. Inert Gas Annealing Treatment of $Ti_3C_2T_x$ MXene Nanosheet

A total of 150 mg of dried $Ti_3C_2T_x$ MXene powder was placed in a tube furnace, heated to 100 °C, 300 °C, 500 °C and 800 °C at a rate of 10 °C /min, then kept for 1 h, and finally

cooled with the furnace. The annealing process was carried out under the protection of a N_2 atmosphere. The black product was ground in a mortar to give product powders, named M_{N_2}-100, M_{N_2}-300, M_{N_2}-500 and M_{N_2}-800. Similarly, the inert gas atmosphere was transformed into Ar and CO_2 gas, and the resulting products were named M_{Ar}-100, M_{Ar}-300, M_{Ar}-500, M_{Ar}-800, M_{CO_2}-100, M_{CO_2}-300, M_{CO_2}-500 and M_{CO_2}-800. The specific treatment conditions and sample names are shown in Table 1.

Table 1. The specific treatment conditions and sample names.

Samples	Treating Temperature/°C	Treating Atmosphere
MXene	-	-
M_{N2}-100	100	N_2
M_{N2}-300	300	
M_{N2}-500	500	
M_{N2}-800	800	
M_{Ar}-100	100	Ar
M_{Ar}-300	300	
M_{Ar}-500	500	
M_{Ar}-800	800	
M_{CO2}-100	100	CO_2
M_{CO2}-300	300	
M_{CO2}-500	500	
M_{CO2}-800	800	

2.4. Characterization

The micro-structure and morphology of the nano-powder prepared were characterized using scanning electron microscopy (SEM, JEOL-JSM7500, JEOL, Tokyo, Japan) and transmission electron microscopy (TEM, JEOL-JEM2100F, JEOL, Tokyo, Japan). The elemental and structural characterization of the products was carried out via X-ray diffraction (XRD, D/MAX 2500, Rigaku, Tokyo, Japan), X-ray photoelectron spectroscopy (XPS, ESCALab220i-XL, VG Scientific, St. Leonards, Britain) and Raman spectroscopy (LabRAM HR Evolution, HORIBA, Paris, France). Thermogravimetric analysis (TGA, STA449F5, NETZSCH, Berlin, Germany) was also conducted for the quantitative analysis of MXene. The dielectric performances of the nanosheets/paraffin composite (mass fraction 30%:70%) in the frequency range of 2–18 GHz were evaluated with a vector network analyzer (CETC AV3672C, Ceyear, Qingdao, China).

3. Results and Discussion

3.1. Characterization of $Ti_3C_2T_x$ MXene

$Ti_3C_2T_x$ MXene nanosheets were prepared by etching the Ti_3AlC_2 MAX phase with a universal LiF-HCl system. After a delaminating process via sonication, accordion-like multilayer MXene tended to transform into a few-layer nanosheet. The typical few-layered morphology which represents the thin-layered structure of $Ti_3C_2T_x$ MXene can be clearly seen in the SEM image (red area in Figure 1a). The successful synthesis of MXene can be verified using XRD patterns (Figure 1b). After etching, a series of characteristic peaks such as the (104) peak of MAX in the MXene plot completely disappeared, while the position of the (002) peak was significantly shifted from 9.6° to 6.6°, indicating that the crystal plane spacing of (002) increases after etching. The XPS spectra (Figure 1c) showed that the Al 2p peak disappeared after etching, proving the elimination of the Al atomic layer. In addition, XPS results showed that the etched MXene contained a large number of O and F atoms, showing the elemental composition of MXene surface functional groups.

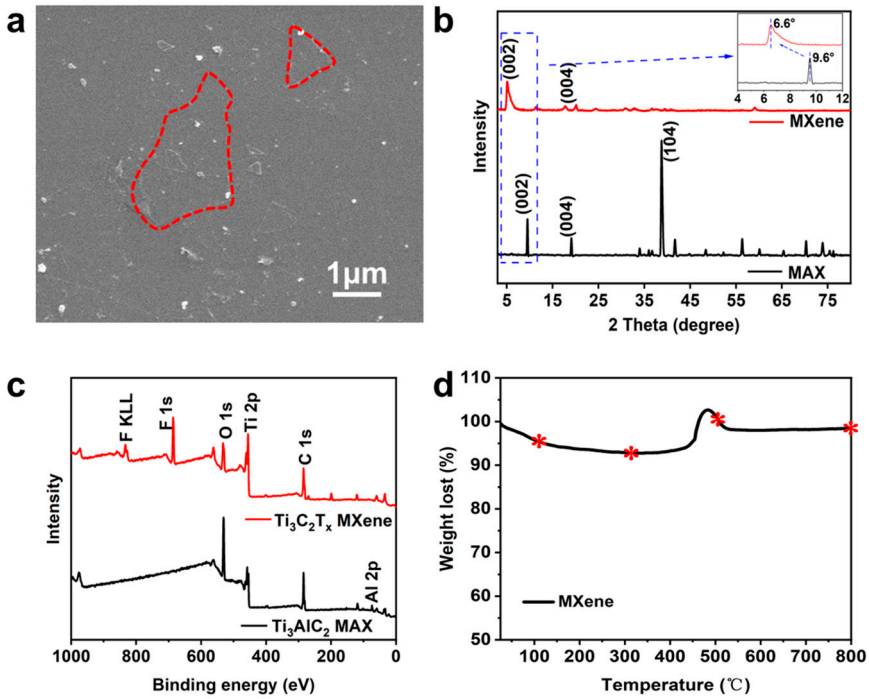


Figure 1. SEM (**a**) image, XRD (**b**) and XPS (**c**) spectra compared to MAX and TG (**d**) spectra of prepared $Ti_3C_2T_x$ MXene. The red area in (**a**) is the layer of $Ti_3C_2T_x$ MXene. The asterisks in (**d**) are the temperature we choose to anneal.

The TG curve of the MXene nanosheet was tested under an air atmosphere as shown in Figure 1d. With the increase in temperature of the air atmosphere, the free H_2O molecules adsorbed in the MXene nanosheet escaped, which was manifested as a loss of mass before 100 °C. As the temperature increased to near 500 °C, the Ti layer in MXene was oxidized to TiO_2 particles, and the C layer was gradually oxidized to CO_2 molecules to escape. The overall performance was that the weight first increased and then decreased. When the temperature was raised to 500–800 °C, the Ti atoms in MXene nanosheets react with O_2 to form TiO_2, while some of the C atoms react with O_2 to form CO_2. However, as the reaction proceeds, all the surface Ti atoms oxidize to the TiO_2 phase, which protects the inner C layer of MXene from further oxidation [22]. Therefore, when annealed in an air atmosphere, MXene exhibits oxidation of the Ti layer and partial destruction of the 2D structure. As a consequence, we chose 100 °C, 300 °C, 500 °C and 800 °C as the characteristic temperatures to explore the inert gas atmosphere annealing treatment. The inert gas atmosphere was chosen to ensure that the C-layer in MXene could not be oxidized during the heating process, thus ensuring the existence of the two-dimensional structure.

3.2. Inert Gas Atmosphere Annealing Treatment

Ti_3AlC_2 MAX was etched into $Ti_3C_2T_x$ MXene with LiF-HCl, and then the product was sonicated to form multilayer MXene nanosheets, which were used to anneal in N_2, Ar and CO_2 atmospheres at different temperatures. X-ray diffraction analysis (XRD) was used to study the crystal structure of the nanosheets after annealing with an inert atmosphere, as shown in Figure 2. A diffraction peak near 6.6° can be seen in each sample, which corresponds to the characteristic peak of the (002) crystal plane of $Ti_3C_2T_x$ MXene. It is worth mentioning that the position of the (002) peak shifted to the left with the increase in treatment temperature under the three inert gases. The position of the characteristic peak is determined by its crystal plane spacing of the (002) plane. The retention of the peak position indicates that the two-dimensional structure of MXene nanosheets after annealing was not destroyed by the annealing treatment. However, the left shift of the peak position indicates an increase in the layer spacing. In addition to the change in peak position,

the area of the (002) peak became wider, indicating that the grain size of the nanosheets became smaller. Except for M_{Ar}-100 (as shown in Figure 2b), the height of the (002) peak was reduced, indicating that the crystal structure was slightly damaged. The higher (002) peak intensity of the M_{Ar}-100 sample may be due to the reduction in defects caused by adsorbed H_2O molecules on the surface of the nanosheet after annealing at 100 °C in the Ar atmosphere, resulting in a more complete crystal structure, while the lower temperature does not destroy the crystal structure.

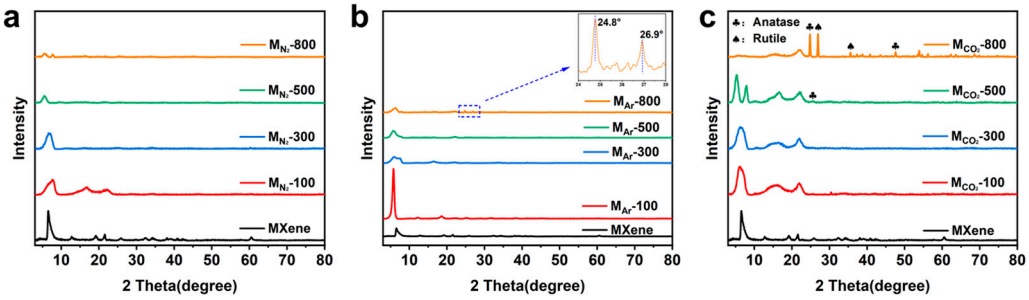


Figure 2. XRD spectra of $Ti_3C_2T_x$ MXene treated with N_2 (**a**), Ar (**b**) and CO_2 (**c**) under different temperatures.

In the XRD patterns of the MXene nanosheets treated in a N_2 atmosphere at different temperatures (Figure 2a), no characteristic peaks of anatase phase and rutile phase TiO_2 were observed, indicating that high temperatures did not oxidize the Ti atomic layer in the N_2 environment. In contrast, the characteristic TiO_2 peaks of anatase (24.8°) and rutile (26.9°) phases appear at 800 °C for MXene nanosheets treated in an Ar atmosphere, as shown in Figure 2b. Similarly, MXene nanosheets treated in a CO_2 atmosphere showed a characteristic peak of anatase phase TiO_2 at 500 °C. At high temperatures, the anatase phase TiO_2 changes to the more stable rutile phase TiO_2. As the temperature increases to 800 °C, the characteristic peak of TiO_2 in the rutile phase appears, and both phases show extremely high peak intensity, as shown in Figure 2c. There was no obvious characteristic TiO_2 peak at 100 °C and 300 °C.

Furthermore, we compared the XRD patterns of the treated M_{N_2}-800, M_{Ar}-800, M_{CO_2}-800 and the original MXene nanosheets at 800 °C, as shown in Figure 3a. Except for the characteristic (002) peak, almost no diffraction peaks representing crystals appeared in the M_{N_2}-800 sample, but the (002) peak became wider and the intensity became lower, indicating that the crystal structure of the nanosheet treated with the N_2 atmosphere at 800 °C was still damaged, but no oxidation of Ti atoms occurred and no new crystals were formed. The (002) peak of the M_{Ar}-800 sample was relatively well retained, and the characteristic peak positions of the anatase phase and rutile phase TiO_2 appeared at the same time, indicating that Ti atoms reacted with O-containing functional groups on the surface. In contrast, the (002) peak of the M_{CO_2}-800 sample almost completely disappeared and was replaced by the strong characteristic peak of anatase and rutile phase TiO_2. In addition to the O-containing functional groups on the surface, CO_2 provides a source of O during the oxidation of Ti atoms. Meanwhile, the original crystal structure of MXene was almost completely destroyed.

To further confirm the above speculation, Raman spectra (the laser wavelength was 633 nm) have been collected and provided in Figure 3b. The A_{1g} (Ti, O, Tx) mode near 201 cm^{-1} (blue dashed line position in Figure 3b), which is the out-of-plane vibration of the outer Ti atoms as well as the carbon and surface groups, could be observed for all samples, confirming that the majority of the sample remains as $Ti_3C_2T_x$ MXene. In particular, the M_{Ar}-800 and M_{CO_2}-800 samples showed vibrational peaks near 151 cm^{-1}, a characteristic peak position for anatase phase oxides of Ti. This is consistent with the results of the previous analysis. For the M_{CO_2}-800 sample, obvious vibrational peaks appeared around 253 cm^{-1}, 421 cm^{-1} and 615 cm^{-1}, which were characteristic peak

positions for the rutile phase oxide of Ti. A weak vibration signal could also be observed in the M_{Ar}-800 sample. We further observed the surface of the sample after observation, and no ablation occurred, which proved that the oxide production was not caused by laser irradiation. This is consistent with the conclusion of XRD. At the same time, the enhancement of the D and G peaks representing the C-layer structure between 1300 and 1600 cm^{-1} of the M_{CO_2}-800 sample indicated a large area of bare leakage in the C-layer. Combined with the attenuation of the signal at 201 cm^{-1} and the enhancement of the oxide signal of Ti, the structure of the M_{CO_2}-800 sample is presumed to evolve into a C-TiO_2 structure. In contrast, the Raman signals of M_{N_2}-800 and MXene were almost identical, which is also consistent with the analytical conclusions of XRD.

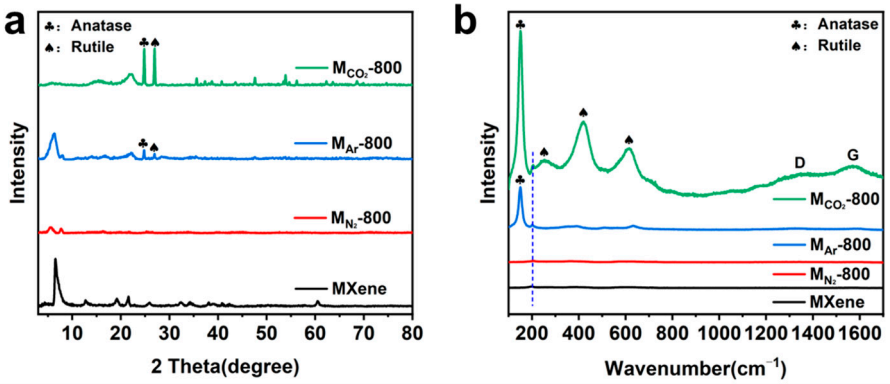


Figure 3. XRD (**a**) and Raman (**b**) spectra of $Ti_3C_2T_x$ MXene treated with N_2, Ar and CO_2 under 800 °C.

X-ray photoelectron spectroscopy (XPS) has been widely used to characterize the surface element content of nanomaterials. The total XPS spectra of samples annealed with a N_2 atmosphere and CO_2 atmosphere at different temperatures are provided in Figure 4a,b. It can be observed in the spectrum that four characteristic peaks are present, corresponding to F 1s, O 1s, Ti 2p and C 1s. The terminal functional group of $Ti_3C_2T_x$ MXene is grafted on the Ti atoms in the surface layer, and its type and content are determined by the etching and post-processing processes. The -OH, =O and -F groups are common termination groups in the products prepared via the LiF-HCl etching process. We restricted the surface functional group composition of the nanosheets to a combination of these three groups in different proportions. It can be seen from Figure 4a,b that the content of F atoms is decreasing. It has been shown that the F-containing functional group does not exist stably at high temperatures, which is consistent with the trend in the figure.

For the M_{N_2} series samples, a clear characteristic peak of N 1s can be observed, which indicates a small amount of N element doping in the sample annealed under a N_2 atmosphere. In order to confirm this point of view, the content of N atoms and Ti atoms are compared and plotted in Figure 4c. It can be seen that with the increase in temperature, the doping amount of N gradually increases from 0.03 to 0.29. In combination with the XRD pattern of Figure 2a, no new crystal characteristic peaks appear, and it is speculated that N elements mainly exist in the M_{N_2} series samples in the way of adsorption. Similarly, in order to confirm that CO_2 participates in the reaction during the processing of M_{CO_2} series samples, the content of O atoms and Ti atoms are compared and plotted in Figure 4d. It can be seen that with the increase in temperature, the content of O increases gradually, from 1.27 to 4.29. The O content did not increase significantly during the low-temperature treatment, indicating that CO_2 was mainly involved in the reaction above 500 °C in this study.

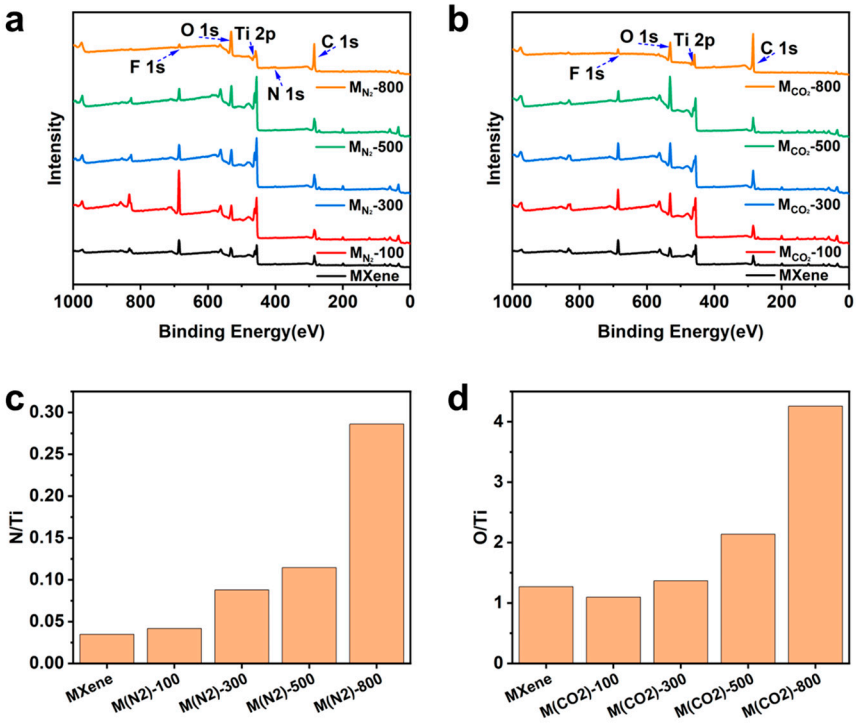


Figure 4. XPS spectra of $Ti_3C_2T_x$ MXene treated with N_2 (**a**) and CO_2 (**b**) under different temperatures; N/Ti ratios of $Ti_3C_2T_x$ MXene treated with N_2 (**c**) and O/Ti ratios treated with CO_2 (**d**) under different temperatures.

We compared the total XPS spectra of the treated M_{N_2}-800, M_{Ar}-800, M_{CO_2}-800 and the original MXene nanosheet, as shown in Figure 5a. The decrease in F after treatment under 800 °C can be clearly observed, indicating that the F-containing functional group on the MXene surface cannot withstand the high temperatures. High-resolution XPS analysis of C 1s peaks was performed for the four samples, and the results are shown in Figure 5b. In M_{N_2}-800, M_{Ar}-800 and raw MXene nanosheets, the C 1s peak can be divided into four secondary peaks located at 281.6 eV, 284.8 eV, 286.9 eV and 288.7 eV, corresponding to C-Ti, C-C, C-O and C=O/C-F bonds, respectively. In the M_{N_2}-800 sample, the C-C bond ratio increased substantially and the C-Ti bond ratio decreased, which we believe is due to the destruction of the layered structure of the nanosheets during the treatment, which corresponds to the loss of the (002) peak in XRD spectra. However, for the M_{Ar}-800 sample, the decrease in the ratio of C-Ti bonds is mainly due to the oxidation of Ti atoms. The process of bonding Ti atoms to O is bound to be accompanied by the breaking of the C-Ti bond. More obviously, C-Ti bonds are hardly observed in the C 1s fine spectrum of the M_{CO_2}-800 sample, supporting the formation of a large amount of TiO_2. Correspondingly, the Ti 2p peaks of the four samples were analyzed using high-resolution XPS, and the results are shown in Figure 5c. In M_{N_2}-800, M_{Ar}-800 and raw MXene nanosheets, Ti 2p peaks can be divided into six secondary peaks located at 454.9 eV, 456.4 eV, 459.2 eV, 461.4 eV, 463.0 eV and 464.9 eV, corresponding to Ti-C $2p^3$, Ti (II) $2p^3$, Ti-O $2p^3$, Ti-C $2p^1$, Ti (II) $2p^1$ and Ti-O $2p^1$ bonds, respectively. Similarly, the large increase in the Ti-O bond ratio in the M_{N_2}-800 sample is due to the destruction of the layered structure of the nanosheets, and the increase in the Ti-O bond ratio in the M_{Ar}-800 sample is mainly due to the oxidation of Ti atoms. This is also supported by the relative content of Ti (II) bonds in the two samples. Similarly, the Ti-C bond almost disappears in the Ti 2p fine spectrum of the M_{CO_2}-800 sample and is replaced by Ti-O. This is consistent with the conclusions of the above analysis.

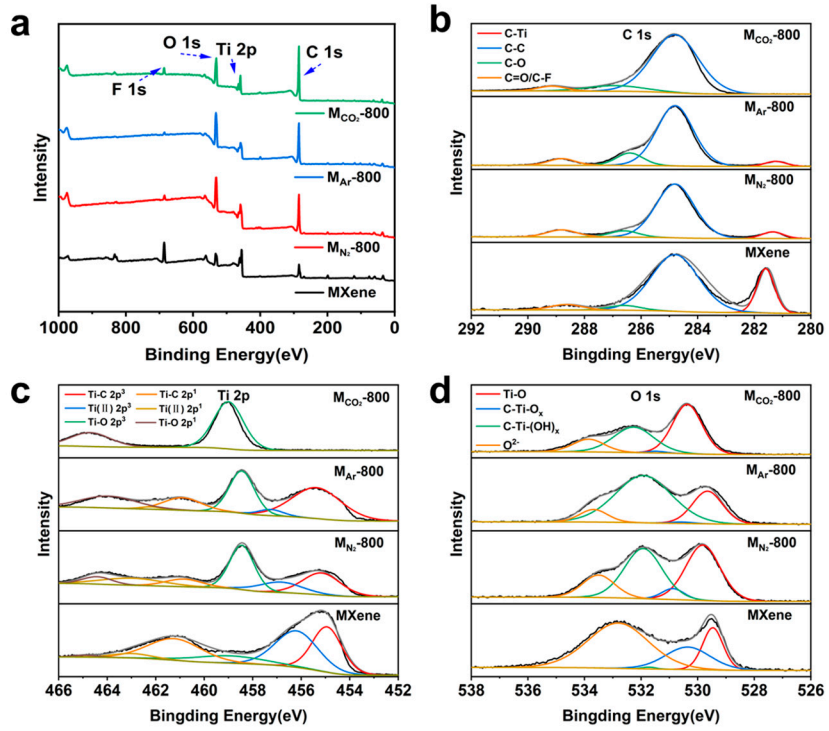


Figure 5. XPS (**a**) spectra and a comparison among high-resolution spectra of C 1s (**b**), Ti 2p (**c**) and O 1s (**d**) of $Ti_3C_2T_x$ MXene treated with N_2, Ar and CO_2 under 800 °C.

High-resolution XPS analysis was used to perform the split-peak fitting of the O 1s peak to further study the existence form and changing trend of O-containing functional groups on the surface, and the results are shown in Figure 5c. The O 1s peak can be divided into four secondary peaks, about Ti-O, C-Ti-O_x, C-Ti- $(OH)_x$ and O^{2-}. In addition, the positions and area ratios of O 1s differentiation peaks are shown in Table 2. It can be seen that compared with pure MXene, the free oxygen contents of M_{N_2}-800, M_{Ar}-800 and M_{CO_2}-800 are significantly decreased, which is inseparable from the effect of temperature. Free oxygen binds to surface Ti atoms to form -OH under the influence of temperature. Meanwhile, the increase in the proportion of Ti-O peaks for M_{Ar}-800 and M_{CO_2}-800 samples was accompanied by a decrease in the proportion of C-Ti-O_x peaks, indicating the formation of TiO_2 after the annealing treatment. In particular, the presence of specific O-valence bonds on the surface of M_{N_2}-800 is closely related to the destruction of the layered structure. The above conclusions are consistent with the aforementioned XRD, Raman and XPS total spectroscopic results.

Table 2. XPS statistics of the peak position and the area ratio of O 1s peaks.

Samples	Position/eV				Area Ratio (α)			
	Ti-O	C-Ti-O_x	C-Ti-$(OH)_x$	O^{2-}	(Ti-O)/[O]	(C-Ti-O_x) /[O]	[C-Ti-$(OH)_x$]/[O]	O^{2-}/[O]
MXene	529.47	530.35	531.72	532.81	0.22	0.12	0.01	0.65
M_{N2}-800	529.81	530.87	531.92	533.50	0.40	0.08	0.36	0.16
M_{Ar}-800	529.65	530.57	531.92	533.68	0.35	0.01	0.50	0.13
M_{CO2}-800	529.90	530.92	532.26	533.85	0.52	0.01	0.37	0.10

The SEM was performed on M_{N_2}-800, M_{Ar}-800 and M_{CO_2}-800, and the results are shown in Figure 6a–c. Figure 6a showed that the M_{N_2}-800 sample size became smaller, and a large number of dark holes existed in the nanosheets, and the two-dimensional structure of the nanosheets was destroyed. Nanoparticles were formed on the surface of the M_{Ar}-800 and M_{CO_2}-800 samples, but not on M_{N_2}-800. The nanoparticles of M_{CO_2}-800

were scanned by HRTEM, and the results are shown in Figure 6d,e. HRTEM image analysis of the two nanoparticles found that Figure 6d showed two lattice stripes with crystal plane spacing of 0.352 nm and 0.184 nm, corresponding to the (101) and (200) crystal planes of the TiO_2 anatase phase. Similarly, Figure 6e shows three lattice stripes with lattice spacing of 0.203 nm, 0.324 nm and 0.230 nm, corresponding to the (210), (110) and (200) crystal facets of the TiO_2 rutile phase, indicating that TiO_2 was generated during the synthesis.

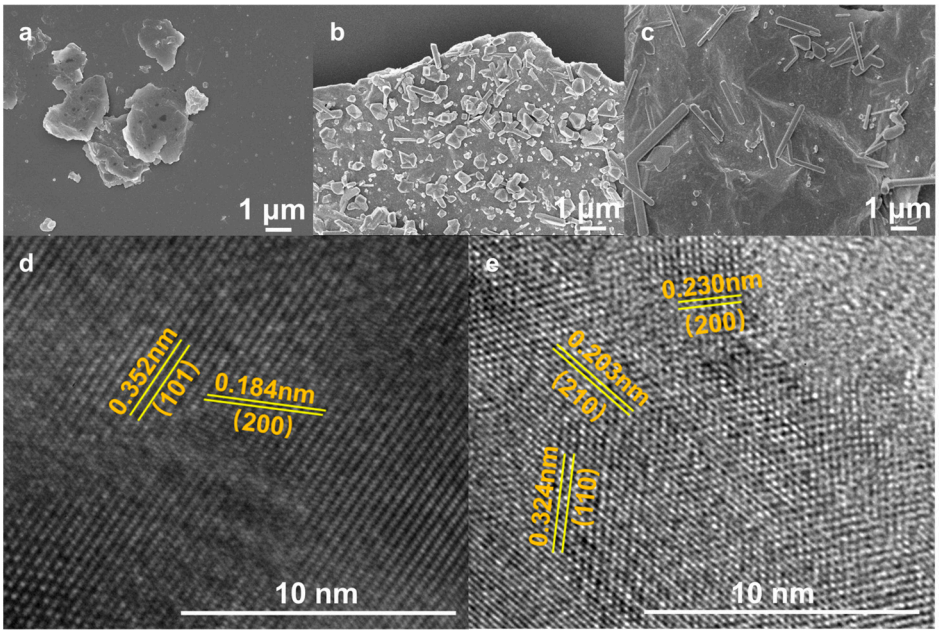


Figure 6. The SEM images of $Ti_3C_2T_x$ MXene treated with N_2 (**a**), Ar (**b**) and CO_2 (**c**) under 800 °C; the HRTEM images of $Ti_3C_2T_x$ MXene treated with CO_2 (**d**,**e**).

The coaxial method was used to characterize the dielectric properties of the samples before and after the inert gas annealing treatment in the form of nanosheets/paraffin composites. The test results for M_{N_2}-800, M_{Ar}-800, M_{CO_2}-800 and the original MXene nanosheets are shown in Figure 7. In general, the dielectric properties of nanosheets are affected by the surface composition and morphology, and the surface functional groups and their positional relationships determine the number and efficiency of polarized channels, which significantly increase the dielectric constant of the composite. The density of samples MXene/paraffin, M_{N_2}-800/paraffin, M_{Ar}-800/paraffin and M_{CO_2}-800/paraffin were 0.25, 0.24, 0.23 and 0.25 $g \cdot cm^{-1}$, respectively. The density values of the four samples were basically the same and had no significant effect on the measurement of dielectric parameters.

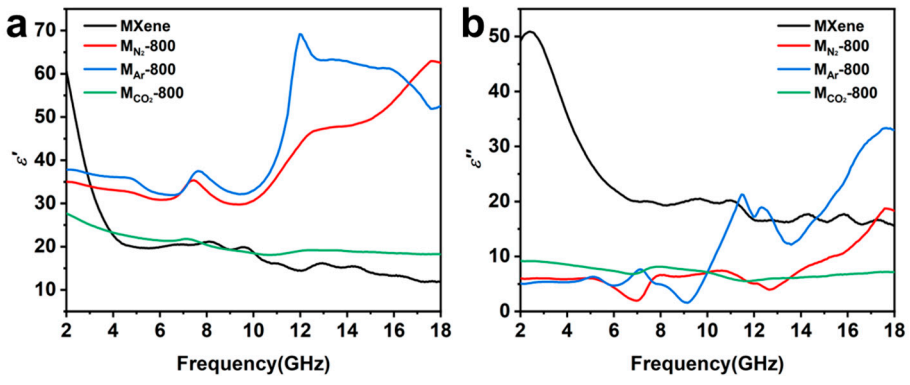


Figure 7. The dielectric performances of $Ti_3C_2T_x$ MXene treated with N_2, Ar and CO_2 under 800 °C: the real part (**a**) and the imaginary part (**b**).

When the external electromagnetic wave reaches, the different types of polarization behaviors caused by the periodic changes in the electromagnetic wave determine the dielectric constant performance of the material, and the size of the dielectric constant determines the energy storage property. In the low-frequency region, due to the slow speed of electromagnetic wave change, the polarization of relatively large grains, ions and other particles can undergo polarization relaxation in response to the change in electromagnetic waves, which then cause the change in dielectric constant. However, in the high-frequency region, particles with large particle sizes cannot respond to the changes in electromagnetic waves in time, and the polarization of electrons becomes the main polarization form. It can be seen from Figure 7a that the lowest permittivity of M_{CO_2}-800 is because the presence of a large number of TiO_2 particles makes it difficult to respond to the changes in electromagnetic waves. At the same time, the large loss of surface functional groups makes the sample unable to respond to the rapidly changing external alternating electromagnetic field in time. Both together lead to the maintenance of the dielectric constant of M_{CO_2}-800 at a low level. The permittivity of pure MXene in the low-frequency region (<4GHz) is extremely high, mainly due to the presence of free oxygen in response to the change in electromagnetic waves. The permittivity of M_{N_2}-800 and M_{Ar}-800 varies similarly with frequency, mainly due to the existence of similar O-containing functional groups on the surface. In the high-frequency region, the dielectric constant of M_{N_2}-800 becomes rapidly higher. This is due to the effect of the N element doped on its surface on the response of the external electromagnetic field. Similarly, the increase in O-containing functional groups (as shown in Table 2) in the M_{Ar}-800 sample led to a rapid increase in the dielectric constant in the high-frequency region. Among them, the small amount of TiO_2 particles on the surface of M_{Ar}-800 causes it to fail to reach the same corresponding level of M_{N_2}-800. The imaginary part of the dielectric constant represents the loss ability of electromagnetic waves in the polarization process, and its variation law is similar to that of the real part of the dielectric constant, as shown in Figure 7b. Using this result, the inert gas atmosphere heat treatment process can be applied to the improvement of the electronic product raw material design.

Based on the above analysis, we can summarize the structural changes of $Ti_3C_2T_x$ MXene after the annealing treatment in an inert gas atmosphere, as shown in Figure 8. Figure 8a shows the two-dimensional nanosheet structure of the original $Ti_3C_2T_x$ MXene. When annealed in a N_2 atmosphere, due to the protective effect, the large area of the Ti atom oxidation behavior will not occur on the MXene surface, but the doping of N element will occur, accompanied by the destruction of the 2D layered structure, as shown in Figure 8b. When annealed in an Ar atmosphere, most of the 2D structure can be effectively preserved. When the temperature is increased to 800 °C, trace oxidation of Ti atoms occurs on the MXene surface, resulting in anatase and rutile phases, as shown in Figure 8c. In the process of annealing in CO_2 atmosphere, anatase phase and rutile phase are formed at 500 °C. When the temperature is increased to 800 °C, the Ti-C bond almost disappears and is replaced by the oxidation of a large number of Ti atoms. In this process, CO_2 participates in the reaction as the source of O, and finally generates the complete C-TiO_2 structure, as shown in Figure 8d. Either treatment is accompanied by the loss of a large amount of F-containing functional groups and the conversion of free oxygen.

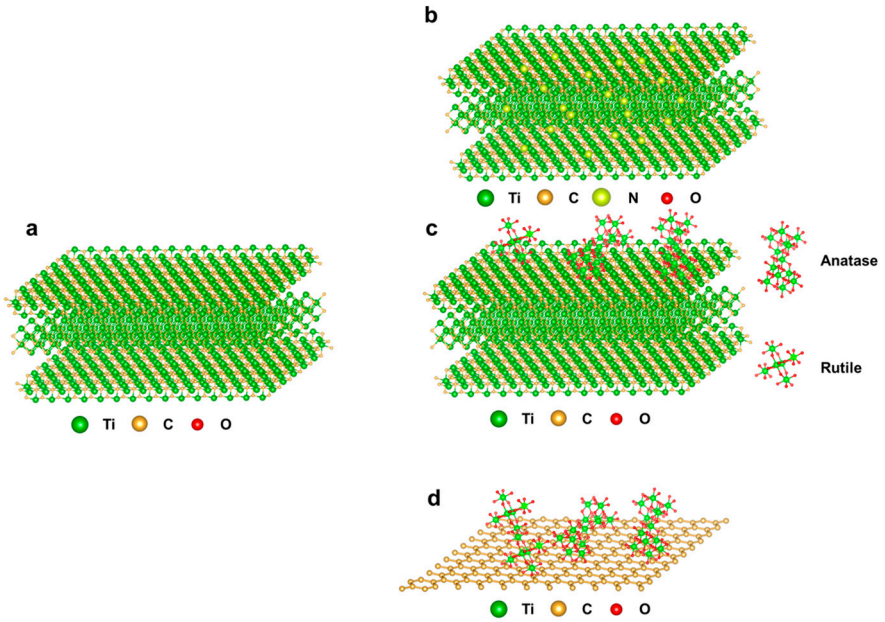


Figure 8. Schematic diagram of structures of $Ti_3C_2T_x$ MXene (**a**) treated with N_2 (**b**), Ar (**c**) and CO_2 (**d**) under 800 °C.

4. Conclusions

In summary, the surface composition and dielectric properties of $Ti_3C_2T_x$ MXene nanosheets were investigated by annealing under inert gas (N_2, Ar and CO_2) atmospheres. XPS results show that the annealing process under an inert gas atmosphere is accompanied by the loss of a large number of F-containing functional groups and the conversion of free oxygen. When annealing in a N_2 atmosphere, N element doping occurs on the surface of MXene, accompanied by the breaking of the two-dimensional layered structure. When annealed in an Ar atmosphere, most of the 2D structure can be preserved. When the temperature is increased to 800 °C, trace oxidation of Ti atoms occurs on the surface of MXene, resulting in anatase phase and rutile. In the process of annealing in a CO_2 atmosphere, anatase phase and rutile phase are formed at 500 °C. When the temperature rises to 800 °C, the oxidized CO_2 of a large number of Ti atoms participates in the reaction as the source of O, and finally generates the complete C-TiO_2 structure. The micro-structure changes have an impact on the dielectric properties of the nanosheets. The mechanism by which the surface micro-structure affects the dielectric properties of nanosheets is elucidated, which provides a broader application field for MXene materials in electronic devices.

Author Contributions: Conceptualization, Z.L. (Zhiwei Liu) and Z.L. (Zhaobo Liu); methodology, Z.L. (Zhiwei Liu); software, Z.L. (Zhaobo Liu); validation, Z.L. (Zhiwei Liu), G.L. and Y.Z.; formal analysis, Z.L. (Zhiwei Liu); investigation, Z.L. (Zhiwei Liu); resources, G.L.; data curation, Z.L. (Zhiwei Liu) and G.L.; writing—original draft preparation, Z.L. (Zhiwei Liu) and Z.L. (Zhaobo Liu); writing—review and editing, Y.Z.; visualization, Z.L. (Zhiwei Liu) and K.W.; supervision, X.C.; project administration, Z.L. (Zhiwei Liu); funding acquisition, Y.Z. All authors have read and agreed to the published version of the manuscript.

Funding: This research received no external funding.

Data Availability Statement: The data presented in this study are available on request from the corresponding author.

Conflicts of Interest: The authors declare no conflict of interest.

References

1. Sinha, A.; Dhanjai; Zhao, H.; Huang, Y.; Lu, X.; Chen, J.; Jain, R. MXene: An emerging material for sensing and biosensing. *Trends Anal. Chem.* **2018**, *105*, 424–435. [CrossRef]
2. Xiong, D.; Li, X.; Bai, Z.; Lu, S. Recent Advances in Layered $Ti_3C_2T_x$ MXene for Electrochemical Energy Storage. *Small* **2018**, *14*, 1703419. [CrossRef]
3. Sun, S.; Liao, C.; Hafez, A.M.; Zhu, H.; Wu, S. Two-dimensional MXenes for energy storage. *Chem. Eng. J.* **2018**, *338*, 27–45. [CrossRef]
4. Yang, J.; Bao, W.; Jaumaux, P.; Zhang, S.; Wang, C.; Wang, G. MXene-Based Composites: Synthesis and Applications in Rechargeable Batteries and Supercapacitors. *Adv. Mater. Interfaces* **2019**, *6*, 1802004. [CrossRef]
5. Li, D.; Lin, Y.; Zhang, M.; Yang, H. Achieved ultrahigh energy storage properties and outstanding charge–discharge performances in $(Na_{0.5}Bi_{0.5})_{0.7}Sr_{0.3}TiO_3$-based ceramics by introducing a linear additive. *Chem. Eng. J.* **2020**, *392*, 123729. [CrossRef]
6. Zheng, B.; Zhu, Q.; Zhao, Y. Fabrication of high-quality silver nanowire conductive film and its application for transparent film heaters. *J. Mater. Sci. Technol.* **2021**, *71*, 221–227. [CrossRef]
7. Li, S.; Fan, Y.; Li, X.; Sun, T.; Liu, Z.; Wang, K.; Zhao, Y. Ultralight hardcarbon nanotubes nanofiber foam/epoxy nanocomposites for comprehensive microwave absorption performance. *Polym. Compos.* **2021**, *42*, 4673–4683. [CrossRef]
8. Wu, F.; Xie, A.; Sun, M.; Wang, Y.; Wang, M. Reduced graphene oxide (RGO) modified spongelike polypyrrole (PPy) aerogel for excellent electromagnetic absorption. *J. Mater. Chem. A* **2015**, *3*, 14358–14369. [CrossRef]
9. Meng, R.; Zhang, T.; Liu, X.; Jiao, P.; Li, J.; Liu, L.; Yuan, Y.; Peng, Q.; He, X. Graphene oxide-assisted Co-sintering synthesis of carbon nanotubes with enhanced electromagnetic wave absorption performance. *Carbon* **2021**, *185*, 186–197. [CrossRef]
10. Deng, B.; Liu, Z.; Pan, F.; Xiang, Z.; Zhang, X.; Lu, W. Electrostatically self-assembled two-dimensional magnetized MXene/hollow Fe_3O_4 nanoparticle hybrids with high electromagnetic absorption performance and improved impendence matching. *J. Mater. Chem. A* **2021**, *9*, 3500–3510. [CrossRef]
11. Liang, L.; Yao, C.; Yan, X.; Feng, Y.; Hao, X.; Zhou, B.; Wang, Y.; Ma, J.; Liu, C.; Shen, C. High-efficiency electromagnetic interference shielding capability of magnetic $Ti_3C_2T_x$ MXene/CNT composite film. *J. Mater. Chem. A* **2021**, *9*, 24560–24570. [CrossRef]
12. Wang, C.; Ma, Y.; Qin, Z.; Wang, J.; Zhong, B. Synthesis of hollow spherical MoS_2@Fe_3O_4-GNs ternary composites with enhanced microwave absorption performance. *Appl. Surf. Sci.* **2021**, *569*, 150812. [CrossRef]
13. Liu, Z.; Cui, Y.; Li, Q.; Zhang, Q.; Zhang, B. Fabrication of folded MXene/MoS_2 composite microspheres with optimal composition and their microwave absorbing properties. *J. Colloid Interface Sci.* **2022**, *607*, 633–644. [CrossRef]
14. Li, S.; Li, Y.; Han, X.; Zhao, X.; Zhao, Y. High-efficiency enhancement on thermal and electrical properties of epoxy nanocomposites with core-shell carbon foam template-coated graphene. *Compos. Part A Appl. Sci. Manuf.* **2019**, *120*, 95–105. [CrossRef]
15. Gao, S.; Wang, G.S.; Guo, L.; Yu, S.H. Tunable and Ultraefficient Microwave Absorption Properties of Trace N-Doped Two-Dimensional Carbon-Based Nanocomposites Loaded with Multi-Rare Earth Oxides. *Small* **2020**, *16*, 1906668. [CrossRef]
16. VahidMohammadi, A.; Rosen, J.; Gogotsi, Y. The world of two-dimensional carbides and nitrides (MXenes). *Science* **2021**, *372*, eabf1581. [CrossRef]
17. Liu, Z.; Zhao, Y.; Li, S.; Sun, T.; Liu, H.; Wang, K.; Chen, X. CeO_2/$Ti_3C_2T_x$ MXene Nanostructures for Microwave Absorption. *ACS Appl. Nano Mater.* **2022**, *5*, 5764–5775. [CrossRef]
18. Wang, Z.; Zhao, P.; He, D.; Cheng, Y.; Liao, L.; Li, S.; Luo, Y.; Peng, Z.; Li, P. Cerium oxide immobilized reduced graphene oxide hybrids with excellent microwave absorbing performance. *Phys. Chem. Chem. Phys.* **2018**, *20*, 14155–14165. [CrossRef]
19. Wu, F.; Xia, Y.; Wang, Y.; Wang, M. Two-step reduction of self-assembed three-dimensional (3D) reduced graphene oxide (RGO)/zinc oxide (ZnO) nanocomposites for electromagnetic absorption. *J. Mater. Chem. A* **2014**, *2*, 20307–20315. [CrossRef]
20. Tang, Q.; Zhou, Z.; Shen, P. Are MXenes Promising Anode Materials for Li Ion Batteries? Computational Studies on Electronic Properties and Li Storage Capability of Ti_3C_2 and $Ti_3C_2X_2$(X = F, OH) Monolayer. *J. Am. Chem. Soc.* **2012**, *134*, 16909–16916. [CrossRef]
21. Tu, S.; Jiang, Q.; Zhang, J.; He, X.; Hedhili, M.N.; Zhang, X.; Alshareef, H.N. Enhancement of Dielectric Permittivity of Ti3C2Tx MXene/Polymer Composites by Controlling Flake Size and Surface Termination. *ACS Appl. Mater. Inter.* **2019**, *11*, 27358–27362. [CrossRef]
22. Li, Z.; Wang, L.; Sun, D.; Zhang, Y.; Liu, B.; Hu, Q.; Zhou, A. Synthesis and thermal stability of two-dimensional carbide MXene Ti_3C_2. *Mater. Sci. Eng. B* **2015**, *191*, 33–40. [CrossRef]

Disclaimer/Publisher's Note: The statements, opinions and data contained in all publications are solely those of the individual author(s) and contributor(s) and not of MDPI and/or the editor(s). MDPI and/or the editor(s) disclaim responsibility for any injury to people or property resulting from any ideas, methods, instructions or products referred to in the content.